SPECIAL ISSUE RESEARCH ARTICLE

INTERNATIONAL JOURNAL OF
ENERGY RESEARCH WILEY

Development of an experimental test rig for cogeneration based on a Stirling engine and a biofuel burner

Luigi Acampora[1] | Gaetano Continillo[2] | Francesco Saverio Marra[1] |
Francesco Miccio[3] | Massimo Urciuolo[1]

[1]Istituto di Ricerche sulla Combustione, CNR, Napoli, Italia, Italy

[2]Dipartimento di Ingegneria, Università del Sannio, Benevento, Italy

[3]Istituto di Scienza e Tecnologia dei Materiali Ceramici, CNR, Faenza, Italy

Correspondence
Francesco Saverio Marra, Istituto di Ricerche sulla Combustione, CNR, via Diocleziano 328, 80124 Napoli, Italy.
Email: marra@irc.cnr.it

Summary

A system consisting of a last-generation Stirling engine (SE) and a fuel burner for distributed power generation has been developed and experimentally investigated. The heat generated by the combustion of two liquid fuels, a standard Diesel fuel and a rapeseed oil, is used as a heat source for the SE, that converts part of the thermal energy into mechanical and then electric energy. The hot head of the SE is kept in direct contact with the flame generated by the burner. The burner operating parameters, designed for Diesel fuel, were changed to make it possible to burn vegetable oils, not suitable for internal combustion engines. The possibility of adopting different configurations of the combustion chamber was taken into account to increase the system efficiency. The preliminary configurations adopted allowed to operate this integrated system, obtaining an electric power up to 4.4 kW_{el} with a net efficiency of 11.6%.

KEYWORDS

biofuel, CHP, distributed power generation, micro-cogeneration, renewable energy, Stirling engine

1 | INTRODUCTION

Distributed power generation in small, decentralized units could help reduce CO_2 emissions, by optimizing the grid capacity and providing opportunities for using locally available renewable fuels.[1]

Recent developments and commercial breakthrough of the Stirling engine (SE) make it available at a scale that is lower than 50 kWel with conversion efficiencies of 25% and more.[2] Free-piston SEs represent the latest and most performing type of such devices, thanks to the absence of a crankshaft with the related mechanical constraint on the motion of the pistons. Thus, the engine design is simpler, resulting in increased efficiency[3] and easier scalability.[4]

Different sources of thermal power may be used for heating the hot exchanger of a SE, including solar,[5,6] natural gas,[7] biomass,[8-11] and waste heat.[12]

A key feature for a cogeneration system, especially for those not connected to a grid system and located in remote regions, is the possibility to run on-demand using a source that can be easily and safely stored for a long time. In this respect, fossil fuels have been the standard source adopted in the past, and their conversion to renewable fuels, mostly derived from locally available biomass, is not straightforward.

Various systems adopting SEs and running on biomasses have been proposed in the past, adopting different conversion technologies. Direct burning of solid biomass in a boiler[13-16] is the simplest option, and improved performances in terms of combustion efficiency, reduced pollutant emissions, and fuel flexibility can be obtained by adopting fluidized bed combustors,[11,17] at the cost of an increased start-up time. Offline production of gaseous fuels, for example, in anaerobic digesters, allows the use of fuel cells[18,19] or innovative gas-fired burners.[19]

Gasification processes are widely adopted in the online conversion of solid biomass, however leading to more complex systems, usually suitable for larger size CHP systems suitable for prolonged run times.[20,21]

Less explored was the possibility to adopt liquid fuels derived from biomass, despite the relative abundance of residual oils coming from the food processing industry, with their LHV being higher than that of most solid and of many gaseous fuels derived from biomass, making transportation and storage relatively easy, and the system ignition on demand easier and more rapid. A comparison of the performances achievable in a cogeneration system based on the coupling of a SE and a burner fed with liquid fuels of fossil or biological source was presented in Reference 22, where the system successfully operated a small scale (1 kWel) SE with a Diesel and biodiesel burner. The feasibility of replacing Diesel with ethanol was proved by Reference 23. In this work, the coupling of a burner fed with vegetable oil in place of Diesel fuel with a medium size SE (up to 7.5 kWel) is proposed.

Rapeseed and sunflower oils may be a valid substitute for fossil Diesel fuel, having similar chemical and physical properties. So far, rapeseed oil is the main feedstock for the preparation of Biodiesel through a trans-esterification step.[24] Biomass pyrolysis can also produce a relevant fraction of liquids, with yield up to 70%wt.[25] However, to be used in industry-standard devices such as IC engines these bio-oils need to be upgraded, to increase their heating value and to remove pollutants.[26] Used cooking oils were also considered as feedstock for the preparation of fuels, needing similar conversion treatments of pyrolysis oils.[27] Conversely, the option to use vegetable, pyrolysis, or used oils as they are in a conventional oil burner would simplify the route for producing energy in small decentralized plants. In this context and under certain conditions (ie, scale lower than 50 kW_el) SEs are optimal candidates to convert the heat generated from fuel combustion into power,[17] being more efficient as compared to other devices (eg, Rankine machines[28] or microturbine and Organic Rankine Cycle[29]).

In general, the hot head of the SE is kept in direct contact with the flame generated by a burner, in order to maximize the thermal exchange between the flame and the working fluid in the engine. This scheme makes it possible to burn oils with characteristics not suitable for internal combustion (IC) engines, for instance not having the viscosity in the range for optimal atomization in Diesel engines. It is worth recalling that the turbulent flame generated by an oil burner upon atomization is very luminous, thus heat transfer to cooling devices via radiation mechanism is predominant.[30]

The article reports on the development of a prototype co-generation system based on a SE and a biofuel burner. The description of the experimental facility and the first results are reported and discussed, along with theoretical speculations for process optimization and further implementation in practical systems.

2 | EXPERIMENTAL METHODS

An experimental test rig was built by coupling a commercial oil burner with a prototype SE. Figure 1 shows a schematic of the experimental facility.

The oil burner (mod. Joannes AZ4 manufactured by FINTERM S.p.A, Italy) is a single stage, atomization flame device, having a maximum nominal power of 50 kW_th. It is equipped with a replaceable nozzle that makes it possible to change the thermal power. The atomization pressure (p_{at}) can be regulated in the range 9 to 12 bar (0.9-1.2 MPa). A fuel tank was installed on an electronic scale for continuously monitoring the oil flow rate to the burner, as shown in Figure 1. Since the burner was designed for a standard Diesel fuel, with the aim of feeding unconventional oils a heated fuel tank (mod. IKA HBR-4) was used with fine pre-heating temperature regulation in the range 20°C to 90°C. A standard automotive Diesel fuel and a rapeseed oil have been adopted during the experiments. The heating value is 42.6 and 38.7 MJ/kg for Diesel and rapeseed oil, respectively.

The exit duct of the burner was mounted at a side of a cylindrical combustion chamber (250 mm inner diameter, 500 mm length) made in AISI 304 and externally insulated with a ceramic blanket. An 80 mm ID exit tube was installed perpendicularly at the opposite side of the chamber (Figure 1) for exhaust evacuation. The total electric consumption of the burner, mostly due to the fuel pumping and air fan, is 0.1 kW_el.

A free-piston SE (QnergymodelPCK80) was adopted in this study, directly converting the reciprocating motion of the piston into electrical power via the integrated linear alternator, with nominal electric power of 7.1 kW_el. The heat exchanger of the SE is made of a bank of U-shaped stainless-steel tubes (Figure 2), able to withstand operation up to 800°C. The whole SE apparatus was enclosed in a cylindrical gas-tight vessel containing the working fluid, helium, at a pressure of 5.2 MPa. A water cooler was also installed for removing the excess heat from the engine. A laboratory equipment was used to provide the water circulation pumping but an ad hoc water circulation circuit provided with a fan coil, following manufacturer instructions, would consume no more than 0.15 kW_el of the produced power.

The exchanger of the SE was installed at the opposite side of the combustion chamber (see Figure 1) and it is in direct contact with the hot gas generated by the burner. The integrated system permitted the adjustment of the distance between the burner and the heat exchanger of

FIGURE 1 Schematic of the experimental facility based on oil burner and Stirling engine [Colour figure can be viewed at wileyonlinelibrary.com]
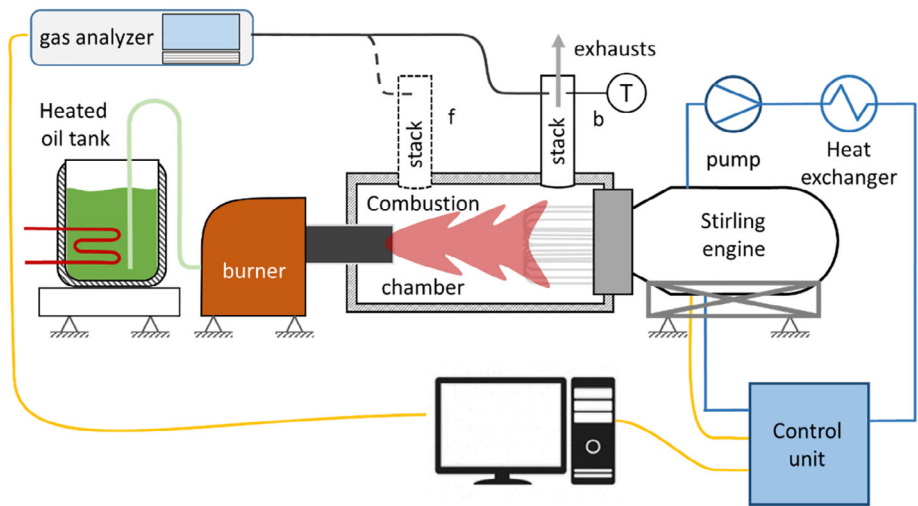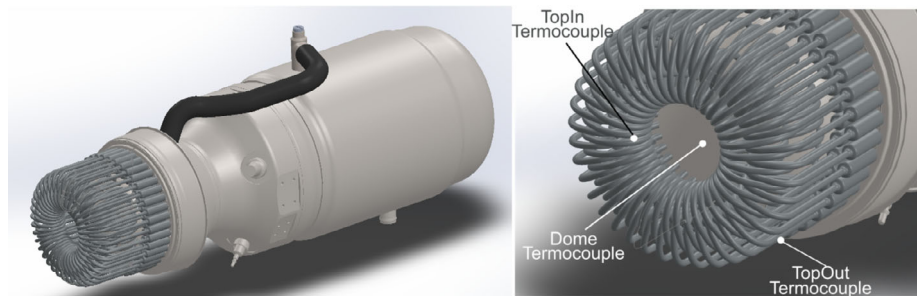

FIGURE 2 Axonometric view of the Stirling engine (mod. Qnergy PCK80.1) with the hot exchanger highlighted in dark grey. The locations of the thermocouples on the exchanger surface are noted at right [Colour figure can be viewed at wileyonlinelibrary.com]

the SE. During the tests, the distance between the exit conduct of the burner and exchanger tubes of the SE was varied from 300 to 400 mm.

Several parameters were continuously monitored during operation and were recorded with a sampling rate of 1 Hz. Three K-type thermocouples recorded the temperature in three different points of the heat exchanger, as shown in Figure 2 by labels 'TopIn', 'TopOut', and 'Dome'.

A K-type thermocouple and a gas probe connected to a continuous gas analyzer (mod. ABB URAS 14) were fitted in the stack for monitoring composition (O_2, CO_2, CO, and NO) and temperature of the exhaust gases.

The temperatures (IN and OUT from the engine, by means of K-type thermocouples) and the mass flow rate (Grunfos VFS 5-100 flow sensor) of the cooling water were also sampled. The engine software interface allowed to monitor the generated power, the generator Current and Voltage, along with Amplitude, Frequency, and Phase of the motion of the piston.

3 | RESULTS

Several tests have been conducted as summarized in Table 1. First, the fuel burner was tested in an open

configuration with both standard Diesel fuel and rapeseed oil. To this aim, a standard type 60° nozzle, denoted as 0.6 GPH, was installed. The atomization pressure was regulated to obtain stable and clean operation of the burner. Particularly, Diesel fuel was injected at $p_{at} = 10$ bar without pre-heating, whilst rapeseed oil required injection at $p_{at} = 12$ barand $T_{pr} = 80°C$. Figure 3 reports a photograph of the flame generated by the burner fired with rapeseed oil, along with a table reporting the composition of the exhaust, averaged over 100 seconds. It appears that the flame covers a total length of around 600 mm and does not expand very much radially.

The exhaust composition was measured by installing the burner in the combustion chamber without the SE. The excess air was around 17%, corresponding to 3.1 vol% in oxygen. CO and NO concentrations are typical values achievable in small oil burners without adopting any countermeasure, such as catalytic conversion or flue gas recirculation.[31] It is worth remarking that the national Italian regulations do not prescribe limits for NO emission in burners below 35 kW$_{th}$, whereas a maximum limit of 1000 ppm of CO normalized at null O_2 concentration is prescribed.[32]

As mentioned above, rapeseed oil required preheating to 80°C and a higher (12 bar vs 10 bar) atomization

TABLE 1 Main parameters and results of experimental tests

Fuel type and conf.[a]	Preliminary tests				Standard tests			
	D-1	D-2	RS-1	RS-2	RSb-1	RSb-2	RSf-1	RSf-2
Burner – Heater distance, mm	400	330	300	300	300	300	300	300
Stack position[a]	b	b	b	b	b	b	f	f
Fuel flow rate, kg/h	2.11	2.19	3.56	3.52	3.10	2.85	3.3	2.6
Nominal Thermal power, kW	24.9	25.9	38.3	37.8	33.3	30.6	35.5	28.0
Excess air ratio,	1.3	1.3	1.17	1.17	1.49	1.63	1.34	1.74
Exhaust temperature, °C	460	520	652	652	613	589	753	653
Electric power, kW	1.75	2.3	4.3	4.4	4.26	3.79	3.74	2.75
Electric efficiency, %	7.0	8.9	11.2	11.6	12.8	12.4	10.5	9.8
Net electric efficiency[b], %	6.0	7.9	10.6	11.0	12.0	11.6	9.8	8.9

[a]D is for diesel, RS is for Rapeseed oil; stack position: b at the bottom, f at the front, of the combustion chamber.
[b]Assuming a conservative estimate of electric consumption by the auxiliary systems of 0.25 kW_{el}.

	average	st. dev.	norm
O2, % vol.	3.1	0.6	0.0
CO2, % vol	13.6	0.3	16.0
CO, ppm	469	161	550
NO, ppm	154	13	181

FIGURE 3 Photograph of the burner flame with rapeseed oil and composition of exhausts on actual and normalized O_2 base [Colour figure can be viewed at wileyonlinelibrary.com]

pressure as compared with fossil Diesel. The liquid fuel temperature was increased to decrease viscosity, as required by the design of the atomizer nozzle. However, this measure most likely affects the vaporization rate as well, which is expectedly higher for the preheated rapeseed oil. This effect certainly has an influence on vaporization and combustion.

Moving from preliminary tests, aimed at verifying the possibility of using renewable rapeseed oil in place of fossil Diesel fuel, to standard tests, aimed at investigating the possibility of optimization of the configuration with rapeseed oil as fuel, the combustion chamber enclosure was sealed and thermally insulated with rock wool lining.

All tests lasted about 10 minutes in order to get, when possible, steady conditions.

3.1 | Preliminary tests

The main operation variables and the results of preliminary tests, carried out in the integrated system with both Diesel fuel and rapeseed oil, are reported in the first four columns of Table 1. Differences were observed because of the indirect influence of the fuel type.

The first two tests (D-1 and D-2) were carried out with slightly different rig configurations: an increased distance between burner and SE of 400 mm was adopted for test D-1, whereas the distance was reduced to 330 mm for test D-2. A partly open combustion chamber on the rear side was used. The large heat losses and the different fluid-dynamic regime, related to the different geometrical configurations, resulted in rather poor performances in terms of generated electricity and efficiency. The system configuration was, hence, modified before carrying out tests with rapeseed oil (RS-1 and RS-2), by closing the combustion chamber, reducing the distance to 300 mm, and improving thermal insulation. Thus, the performance of the system was substantially improved, as discussed in the following paragraph.

Figures 4 and 5 report, for tests D-1 and D-2, the measured time series of the main thermal, mechanical, and electric variables. More specifically, each subfigure reports input and output temperatures of the coolant (on the left), temperatures in three points of the heater, along with the average value (on the right), respectively.

Test conditions were varied, over successive runs, in order to obtain a stable flame. It was observed that a stable flame, that is, a flame associated with a monotone sound coming from the combustion chamber, yields stable regime temperatures and electric power.
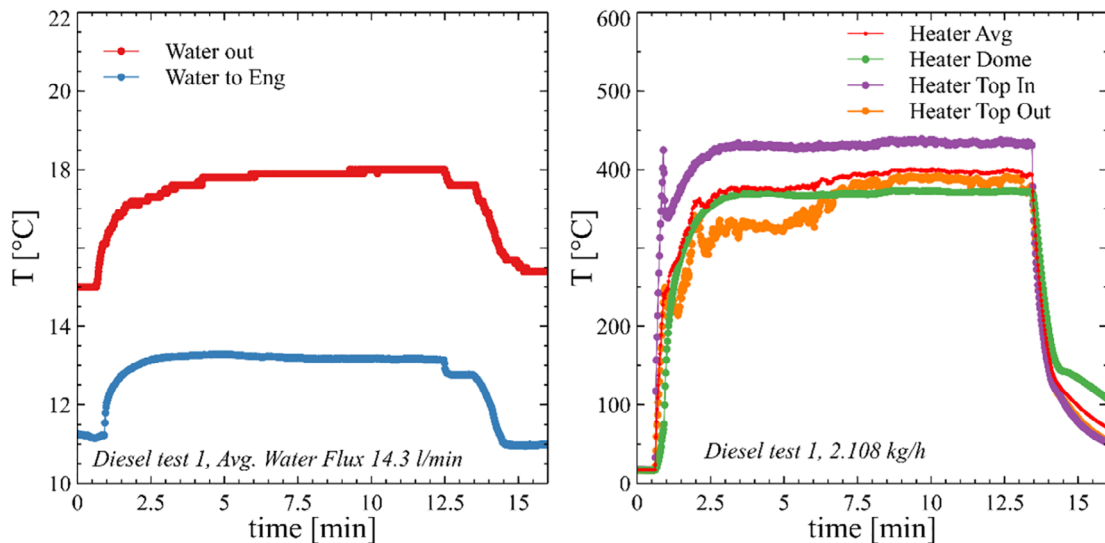
FIGURE 4 Temporal profiles of temperatures (test D-1) [Colour figure can be viewed at wileyonlinelibrary.com]
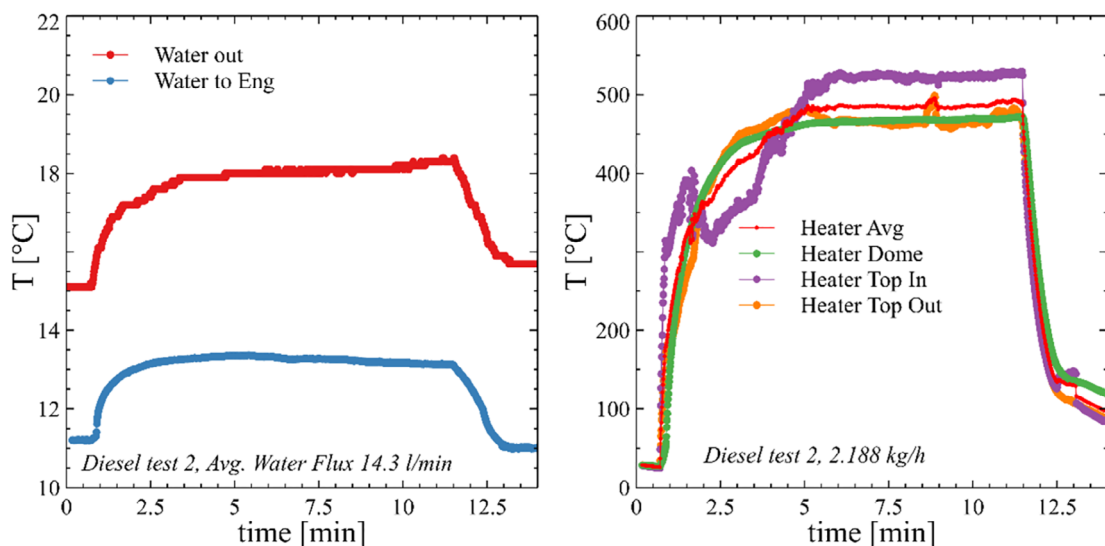

FIGURE 5 Temporal profiles of temperatures (test D-2) [Colour figure can be viewed at wileyonlinelibrary.com]

Typical temporal profiles of temperature show a first transient stage during which temperature increases rapidly (see Figures 4 and 5). Temperature distribution on the heater of the engine was not uniform and took some time to stabilize until, after about 2 minutes, the homogeneous heating of all components was achieved. A second effect is clearly observable in Figures 4 and 5: from test D-1 to test D-2 the length of the combustion chamber was decreased, leading to a closer contact of the flame with the engine heater. In this way, higher values of the average temperatures on the heater surface (from 400°C, Figure 4 right, to 485°C, Figure 5 right) were achieved. The configuration with a reduced length has led to an

increase of the electric power from 1720 to 2360 W, as observed in Figure 6.With an increase of the electric power, the transient required to reach a constant output power becomes longer, correlated to the increased cooling of the SE head, especially in the region of the dome.

The second round of tests, reported in Figures 7–9 was conducted with the rapeseed oil. In this case, the nominal thermal power (the mass flow rate multiplied by the Lower Heating Value of the fuel) was significantly higher than in the previous tests, thanks to the increase of the injection pressure. These two tests were performed in an almost identical configuration, the only difference
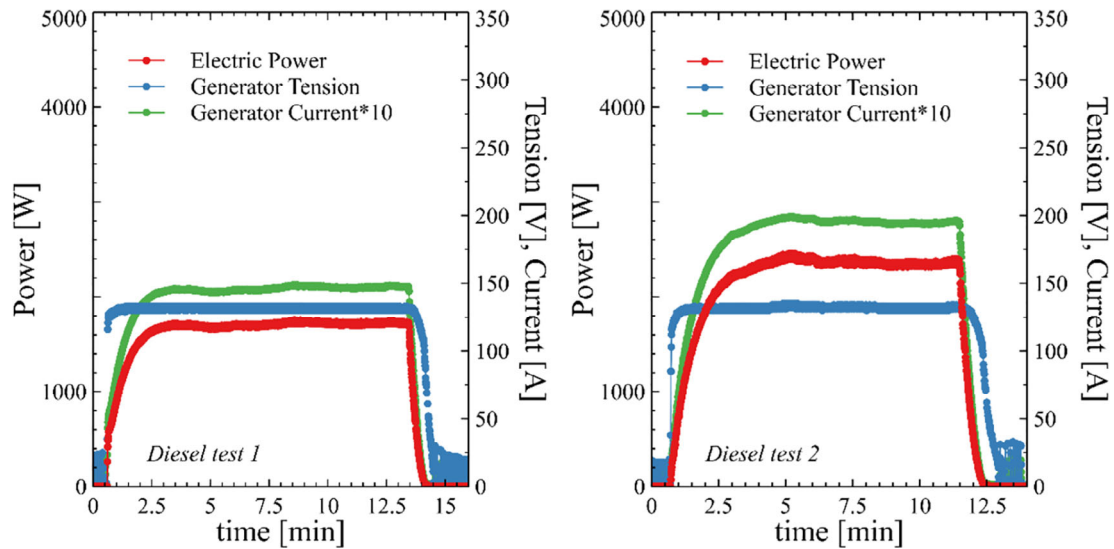
FIGURE 6 Temporal profiles of electric quantities. Left: test D-1; right: test D-2 [Colour figure can be viewed at wileyonlinelibrary.com]
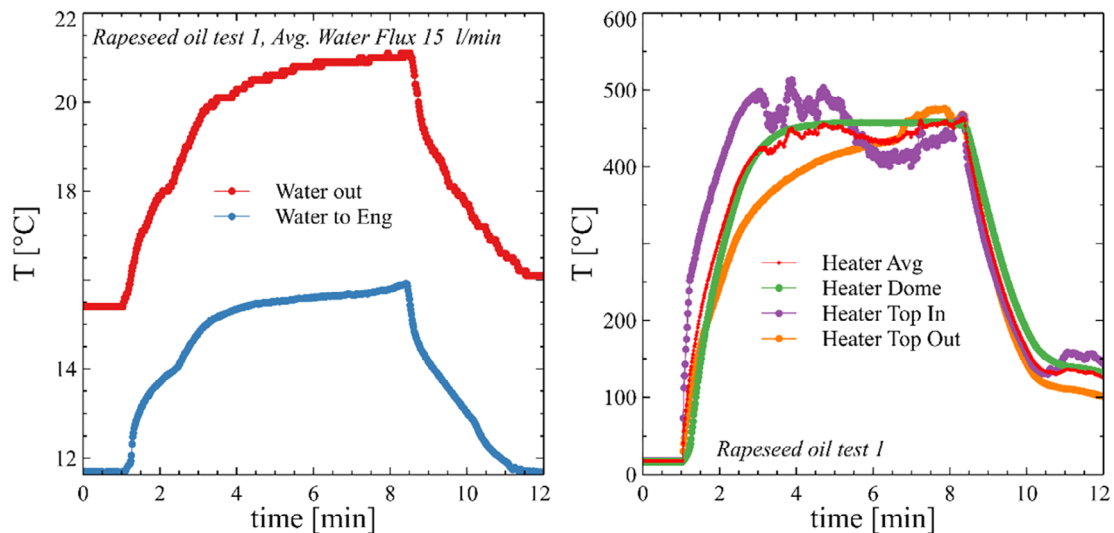

FIGURE 7 Temporal profiles of temperatures (test RS-1) [Colour figure can be viewed at wileyonlinelibrary.com]

being the addition of an external draught on the exhaust pipe. A reduced length of 300 mm for the combustion chamber was adopted for both tests with rapeseed oil.

The temperature profiles on the surface of the heater show marked instabilities during the first run conducted starting from cold conditions (see Figure 7, right). The second test was conducted at short delay from the previous. The added draught clearly helped stabilize the flow field in the combustion chamber leading to a uniform trend of the temperatures. In both cases, the transient, thanks to the increased power, was slightly reduced with respect to test with Diesel starting from cold conditions, and further reduced to 1 minute in the case of re-ignition after preheating from the previous run.

Despite the instabilities on the temporal profile of temperature in the first test, the power generated was very similar in the two tests.

By increasing the nominal thermal power from 25 to 38 kW, the electric power generated increased from 2360 to 4470 W (see Figures 6 and 9), thus leading to a significant increment of the efficiency.

Figure 10 reports mechanical quantities related to the motion of the free piston, that is, frequency, amplitude, and phase. It appears that the engine reacts to the increase of the power input by mainly changing the amplitude of the oscillations while keeping the frequency constant. The irregular time behavior of the temperature on the heater surface, having two different stages in test
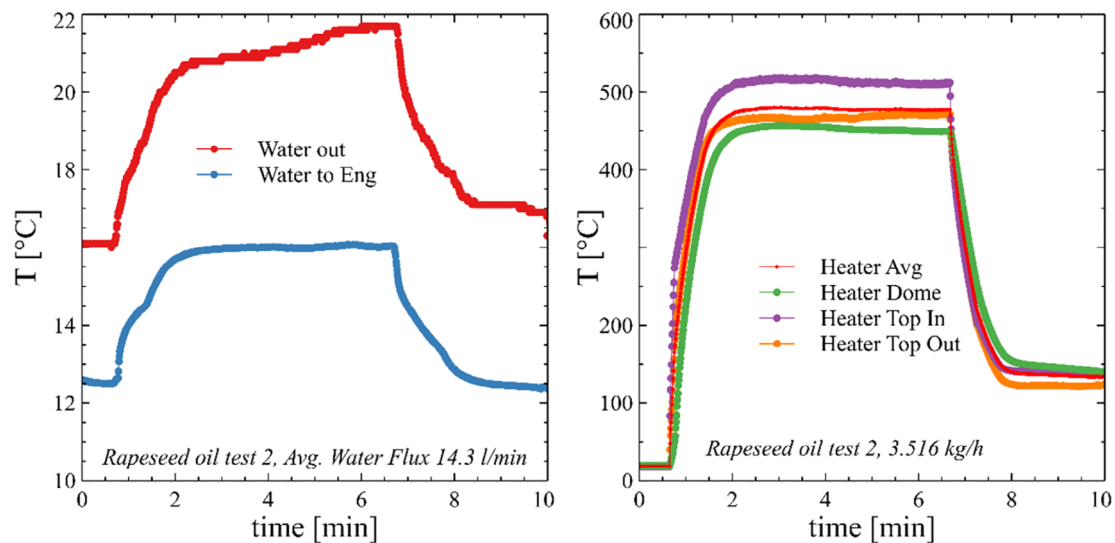
FIGURE 8 Temporal profiles of temperatures (test RS-2) [Colour figure can be viewed at wileyonlinelibrary.com]
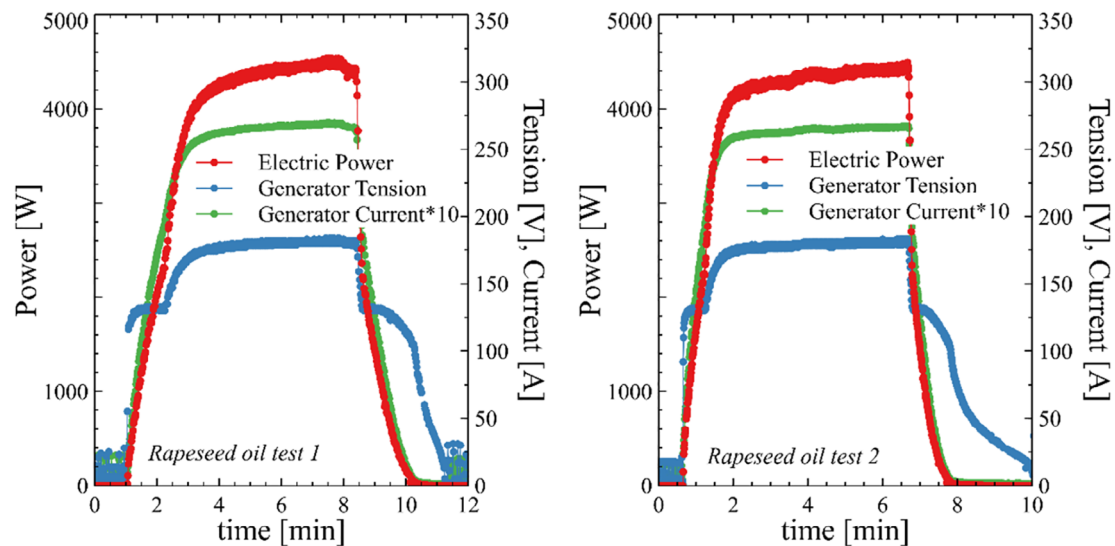

FIGURE 9 Temporal profiles of electric quantities (tests RS-1 and RS-2) [Colour figure can be viewed at wileyonlinelibrary.com]

RS-1 and a regular behavior in test RS-2, appears to influence the phase angle between piston and displacer.

3.2 | Effect of the fuel flow rate

Tests were conducted with rapeseed oil to study the effect of the fuel flow rate, by comparing the performance attained with two values of the flow rate for both positions of the exhaust gas stack, that is, tests RSb-1 vs RSb-2 and RSf-1 vs RSf-2, as summarized in Table 1 (see also Figure 1). It is to be noted that the fan providing the necessary air supply was not regulated, and therefore a

different equivalence ratio was reached in each test, with the excess air increasing by decreasing the fuel feed rate, from 1.49 to 1.63 for tests RSb and from 1.34 to 1.74 for tests RSf. This affected directly the maximum temperature in the heater zone, as well as the temperature of the exhaust gases. Higher temperatures mean lower gas density, and this affects the residence time of the hot gases in the heater zone, resulting in a favorable increase of the heat transfer rate achieved at lower air excess ratios. As a result, the electric power produced in the two conditions changed from 4.26 to 3.79 kW_{el} in test RSb-1 and RSb-2 respectively, and from 3.74 to 2.75 kW_{el} in tests RSf-1 and RSf-2, respectively. These decrements compare well with
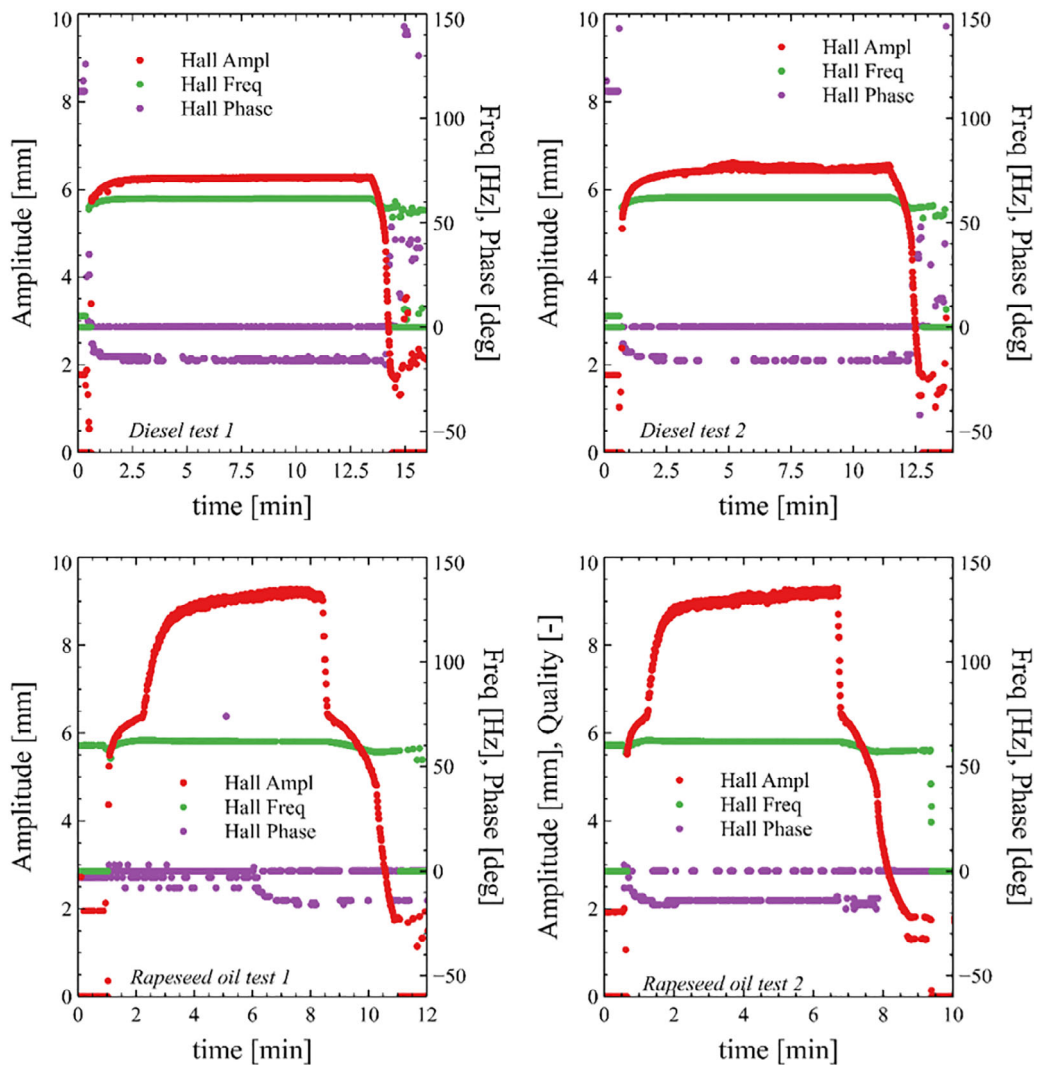
FIGURE 10 Kinematics of the motion of the free piston engine (all preliminary tests) [Colour figure can be viewed at wileyonlinelibrary.com]

the temperature difference that can be estimated between the theoretical adiabatic flame temperature and the measured exhaust gases temperature in each of the tests performed, which read 1075 and 962 in tests RSb-1 and RSb-2, and 1116 and 807 in tests RSf-1 and RSf-2, respectively.

Inspection of the emission profiles, reported in Figures 11 and 12, and corresponding average values reported in Table 2, confirms the higher consumption of oxygen for tests with higher fuel flow rates, remaining in overall lean fuel feed conditions. These profiles also show that emissions of nitrogen oxides are very low (in the range of 25-55 ppm). CO emissions are almost constant around 550 ppm for tests RSb, much lower in test RSf-1 (around 60 ppm), and much larger in test RSf-2. In the latter test, the burner started to experience unstable conditions prone to burn-off, because of the low fuel flow rate.

3.3 | Effect of the position of the exhaust stack

Further tests, by fueling rapeseed oil, were conducted to study the effect of the position of the stack. Its original position, located in the back of the combustion chamber (b) practically immediately on top of the engine heater, was moved close to the front of the combustion chamber (f), above the burner injector (see Figure 1). For each of the two configurations, two different fuel feed rates were adopted, as summarized in Table 1.

It results that better performances were obtained with configuration b. This was especially evident in the values of the electric power produced, that decreased from 4.27 to 3.74 kW$_{el}$ at the higher fuel feed rates (around 3.2 kg/h) and from 3.79 to 2.75 kW$_{el}$ at the lower fuel feed rates (around 2.7 kg/h). The flow field inside the combustion chamber was strongly affected by the stack
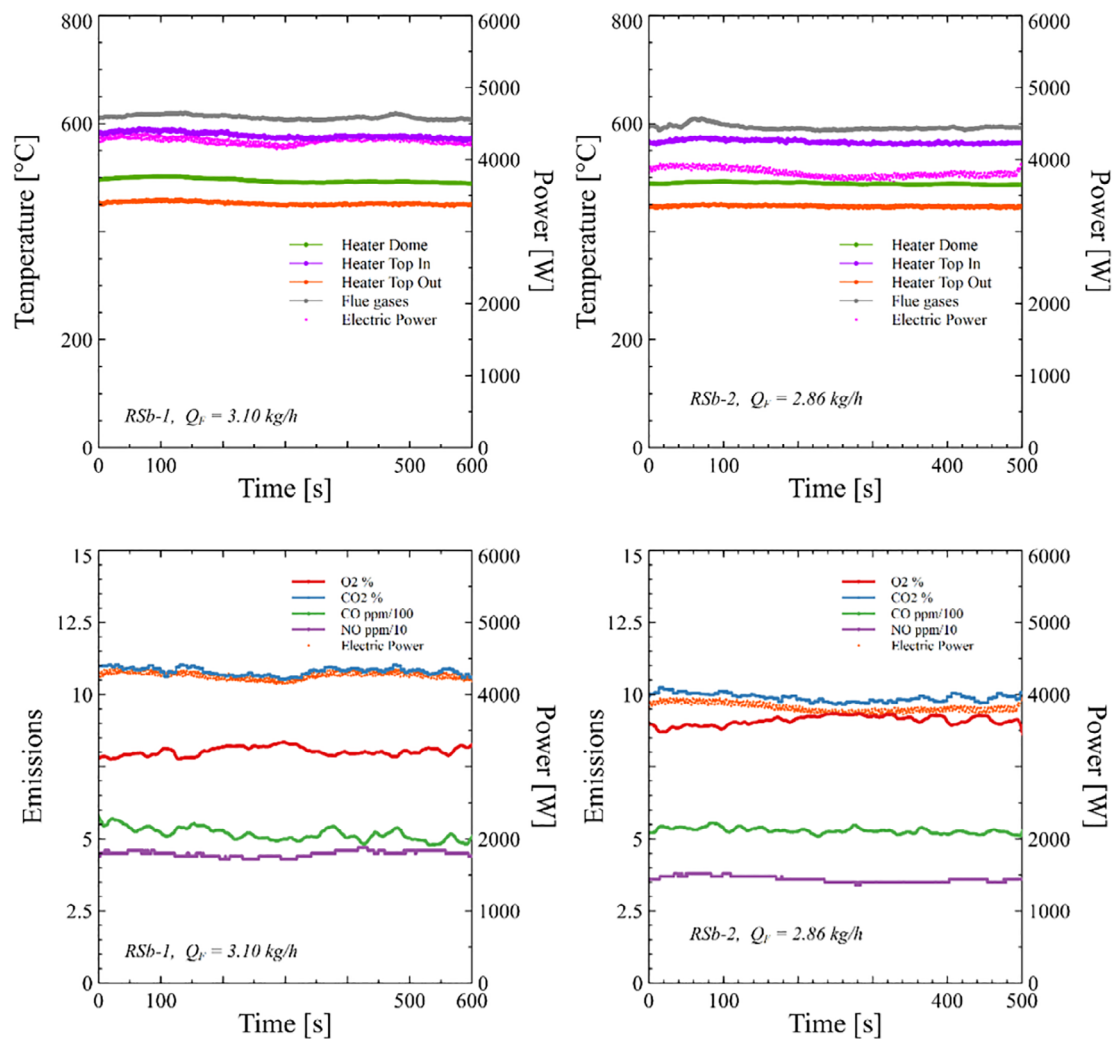
FIGURE 11 Temperature in the heater zone and exhaust stack (top pictures) and emissions measured in tests RSb-1 (left column) and RSb-2 (right column) [Colour figure can be viewed at wileyonlinelibrary.com]

position. Indeed, the exhaust gases left the combustion chamber at a much higher temperature if the stack was in position f (753°C in test RSf-1 vs 613°C in test RSb-1 and 653°C in test RSf-2 vs 589°C in test RSb-2), meaning that some of the hot gases formed in the first portion of the flame followed a direct path towards the stack, without crossing the tubes of the heater. This phenomenon lead to a loss of power transferred to the engine, despite the higher temperatures measured on the heater of the SE in configuration RSf-1 (524°C) vs those in configuration RSb-1 (493°C). Furthermore, the large increase in CO concentration during the test RSb-1 is a proof that combustion was unsteady, probably due to the accumulation of the fuel droplets on the internal surface of the combustion chamber, followed by slow and incomplete combustion of fuel vapors. On the whole, the result underlines the importance of reaching both thermal and flow conditions able to promote favorable mechanisms of

heat transfer between the flame and the tubes of the heater, as well as good combustion behavior.

4 | DISCUSSION

The results illustrated above indicate a real possibility to adopt a SE to cogenerate heat and electric power in a very simple way. To estimate the possible use of the two shares of energy (thermal and electric), a further analysis is required. The recorded data allow an estimate of the main contributions to the energy balance of the system. Four main outcomes of the thermal power delivered by the combustion of the fed fuel can be identified: the power converted into electricity, the power that leaves the system with the flue gas, the thermal power dissipated by the engine into the cooling water and the power that is dissipated to the environment. Of the last two shares of thermal
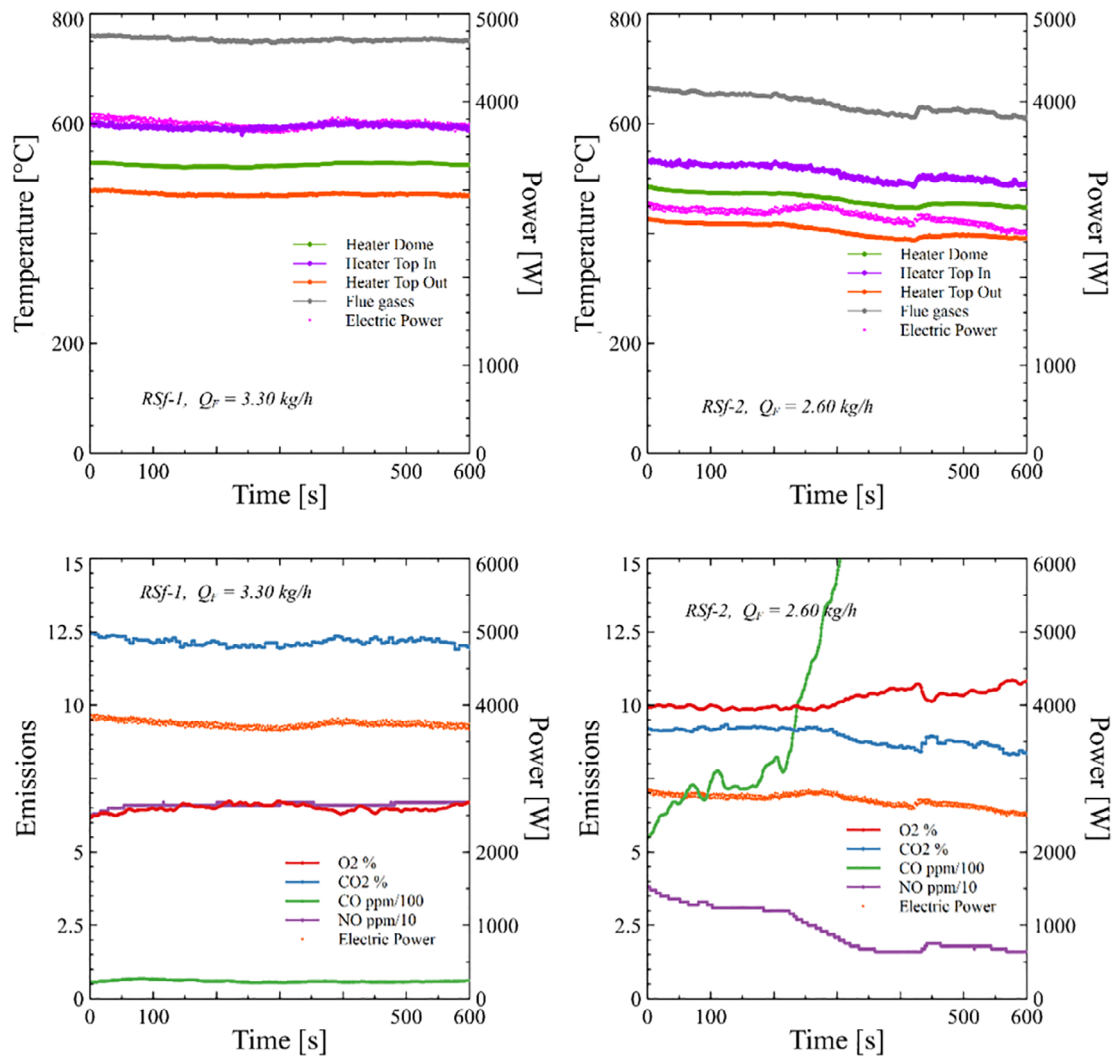
FIGURE 12 Temperature in the heater zone and exhaust stack (top pictures) and emissions measured in tests RSf-1 (left column) and RSf-2 (right column) [Colour figure can be viewed at wileyonlinelibrary.com]

TABLE 2 Average measured emissions during tests with rapeseed oil

	RSb-1			RSb-2			RSf-1			RSf-2		
	Average	St. dev.	Norm.	Average	St. dev.	Norm.	Average	St. dev.	Norm.	Average	St. dev.	Norm.
O_2, % vol.	8.0	0.1	0	9.1	0.2	0	6.5	0.1	0	10.2	0.3	0
CO_2, % vol	10.8	0.1	17.5	9.9	0.1	17.5	12.2	0.1	17.6	8.9	0.3	17.3
CO, ppm	522	24	845	530	9	935	60	4	87	1320	533	2563
NO, ppm	45	1	72	36	1	64	66	1	96	24	7	46

power, the one dissipated to the environment cannot be recovered for further use and is therefore to be considered a net loss of energy. The power dissipated into the cooling water, depending on the specific installation and on the temperature reached by the water, may be adopted, for instance, for ambient heating. It should be noted that an increase in the temperature can be easily obtained by reducing the flux of cooling water, but the effect on the engine efficiency can be significant and need to be considered. Therefore, this yield may be considered a loss as well as a low enthalpy recoverable share.

The four fractions of energy were directly measured, as for the generated electric power, or indirectly measured or estimated as explained in the following.

FIGURE 13 Share of thermal and electric power in the preliminary experimental tests [Colour figure can be viewed at wileyonlinelibrary.com]
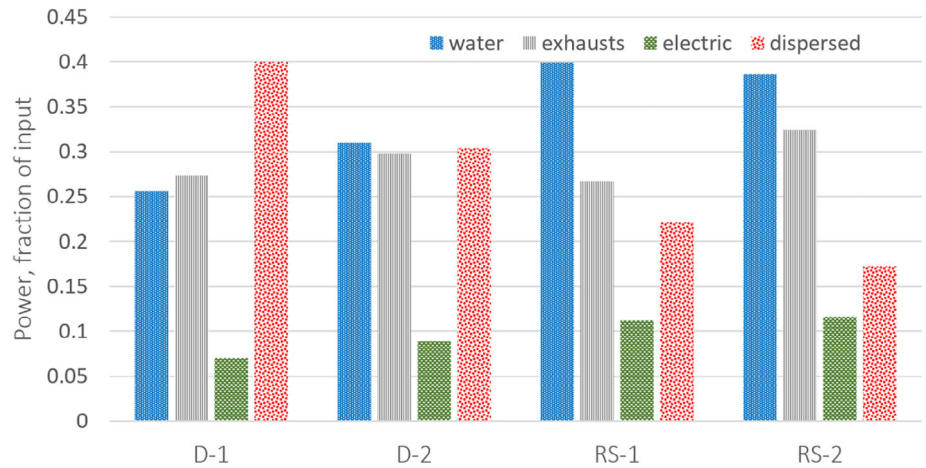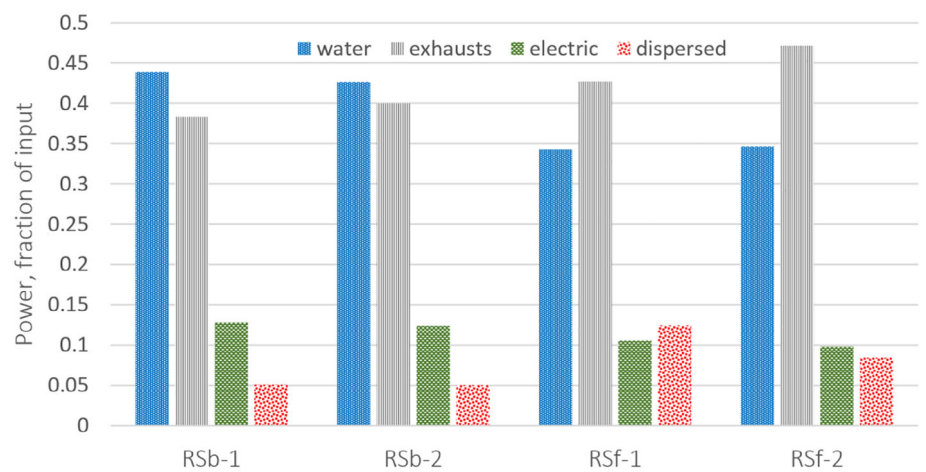

FIGURE 14 Share of thermal and electric power in the final experimental tests [Colour figure can be viewed at wileyonlinelibrary.com]

The thermal power leaving the system with the flue gases was computed knowing the exhaust gas temperature T_{exh}, assuming for the specific heat of the exhaust gas, $C_{p,\,exh}$, the value of 1.2 J/(kg K), and evaluating the total mass of flue gases, given by the mass flow rate of inlet fuel, $\dot{M}_{fuel}$ directly measured, and the mass flow rate of air estimated as $\dot{M}_{air} = \dot{M}_{fuel}(1 + A_E)A_S$, being A_E the excess air adopted by the burner and A_S the stoichiometric air fuel ratio. Table 2 reports the relevant data for all the tests performed.

The thermal power leaving the system was computed as:

$$P_{exh} = C_{p,exh}\left(\dot{M}_{air} + \dot{M}_{fuel}\right)\left(T_{exh} - T_{ref}\right)$$

The thermal power leaving the engine with the cooling water, P_{cool}, was simply estimated as the difference between the heat that enters the engine, P_{heat}, and the electric power generated P_{el}. The first one was estimated starting from the performance charts of the engine, determined by the engine manufacturer, that

report the electric power produced for a given amount of heat transferred to the engine, parametrized by a temperature index.[33] Then:

$$P_{cool} = P_{heat} - P_{el}$$

Finally, being $P_{comb} = \dot{M}_{fuel}LHV$ the heat produced by the combustion of the fuel and $P_{in} = C_{p,air}\dot{M}_{air}(T_{amb} - T_{ref}) + C_{p,fuel}\dot{M}_{fuel}(T_{fuel} - T_{ref})$ the power entering with the inlet mass fluxes of air (at ambient temperature T_{amb}) and of fuel (at the preheating temperature T_{fuel}), the dispersed power is computed as:

$$P_{disp} = P_{in} + P_{comb} - P_{el} - P_{exh} - P_{cool}$$

Figure 13 shows the relative distribution among thermal (water, exhaust, and dispersed) power and electric power for the four preliminary tests reported in Table 1.

Apart from the decrease of the dispersed power moving from D-1/D-2 to RS-1/RS-2, as a consequence of the above reported plant improvement, it can be noted that the sensible heat of the exhaust increases in tests RS-1 and RS-2, operated

at higher total power. Under these conditions, the higher exhaust temperature allows obtaining increased SE efficiency and electric power, but the losses with exhaust also increase.

Similar results as those presented in Figure 13 are shown in Figure 14 for the standard tests with rapeseed oil. The effect of a better insulation of the chamber is clearly recognized in the much lower amount of the fraction of dispersed energy that is common to all standard tests with respect to preliminary tests. The effect of the stack position is recognized in the switch of the maximum fraction of the end share of energy between those in the water, maximum with the stack above the heater, and those in the exhaust gases, maximum with the stack above the burner. It is noticeable that the increase of energy yield in the exhaust also increases the dispersed share of energy: not only more energy is lost with the combustion fumes, but also the absorbed energy is used with less efficiency. Consequently, a larger electric power is always produced in the first configuration of the stack.

5 | CONCLUSIONS

An integrated oil-burner and SE system was developed and assembled based on commercially available devices that have been operated in conditions different from their standard specifications. The integrated system was successfully fired with vegetable oil (rapeseed) obtaining an electric power up to 4.4 kW_{el} and maximum net efficiency, P_{el}/P_{comb}, of 12.8%.

Even if these results are far from optimal, they demonstrate the feasibility of using a renewable liquid fuel to provide heat to a SE via a standard spray burner. Further research on the optimization of the combustion chamber design will be planned for improving the global efficiency of the integrated co-generation system.

Some directions have already been investigated. Different configurations of the combustion chamber were adopted to reduce the heat dispersed with the exhaust gases, especially if the increase in yield of electric energy is desired. Improved insulation of the combustion chamber leads to a significant decrease in the energy dispersed. Also, the configuration of the flow field inside the combustion chamber was found to be very important to promote a favorable mechanism of heat transfer with the heater and to avoid direct loss of energy from that portion of hot gases directly reaching the stack without interacting with the SE heater. Also important was found the distance of the burner from the SE heat exchanger: a further decrease of this distance is probably beneficial to increasing the electric power produced.

Other aspects need further development, also including detailed numerical modeling. The flame dynamics is certainly affected by the several parameters investigated, and a deeper investigation of this aspect would reveal effects enlightening space for further improvement of heat transfer to the SE, reduction of pollutant emissions, improved combustion efficiency, especially if coupled with an investigation of the available settings of the burner.

NOMENCLATURE

A_E	excess airadopted by the burner
A_S	stoichiometric air fuel ratio
C_p	specific heat at constant pressure
LHV	lower heating value
$\dot{M}$	mass flow rate
p_{at}	atomization pressure
P_{comb}	heat produced by the combustion of the fuel
P_{cool}	thermal power leaving the engine with the cooling water
P_{disp}	dispersed power
$P_{el.}$	electric power generated
P_{exh}	thermal power leaving the system
P_{heat}	heat that enters the engine
P_{in}	power entering with the inlet mass fluxes of air (at temperature T_{amb}) and of fuel (at temperature T_{fuel})
T	temperature
T_{amb}	ambient temperature
T_{ref}	reference temperature (298.15 K)

SUBSCRIPT

air	air
fuel	fuel
exh	exhaust

ORCID
Luigi Acampora https://orcid.org/0000-0002-0031-1058
Gaetano Continillo https://orcid.org/0000-0002-6012-3999
Francesco Saverio Marra https://orcid.org/0000-0003-4231-5652
Francesco Miccio https://orcid.org/0000-0003-0643-6721
Massimo Urciuolo https://orcid.org/0000-0002-9386-3053

REFERENCES
1. Pehnt M. Environmental impacts of distributed energy systems—the case of micro cogeneration. *Environ Sci Pol*. 2008; 11:25-37.

2. Walker F. *Stirling Engines*. Oxford, UK: Clarendon Press; 1980.

3. Breeze P. Chapter 6—Stirling engines and free piston engines. In: Breeze P, ed. *Piston Engine-Based Power Plants*. London, England: Academic Press; 2018:59-70.

4. Sowale A, Kolios AJ. Thermodynamic performance of heat exchangers in a free piston Stirling engine. *Energies*. 2018;11:505.

5. Kongtragool B, Wongwises S. A review of solar-powered Stirling engines and low temperature differential Stirling engines. *Renew Sust Energ Rev*. 2003;7:131-154.

6. Singh UR, Kumar A. Review on solar Stirling engine: development and performance. *Therm Sci Eng Prog*. 2018;8:244-256.

7. Thorsen JE, Bovin J, Carlsen H. 3 kW Stirling engine for power and heat production, IECEC 96. *Proceedings of the 31st Intersociety Energy Conversion Engineering Conference*. Vol 2. Washington, DC: IEEE; 1996:1289-1294. https://doi.org/10.1109/IECEC.1996.553902.

8. Podesser E. Electricity production in rural villages with a biomass Stirling engine. *Renew Energy*. 1999;16:1049-1052.

9. Cardozo E, Erlich C, Malmquist A, Alejo L. Integration of a wood pellet burner and a Stirling engine to produce residential heat and power. *Appl Therm Eng*. 2014;73:671-680.

10. Chirone R, Marra FS, Miccio F, Miccio M, Solimene R, Urciuolo M. Integrated fluidized bed combustor and Stirling engine for micro-scale cogeneration, Proceedings of the 23rd International Conference on Fluidized Bed Conversion. Seoul; 2018:937-947.

11. Urciuolo M, Chirone R, Marra FS, Solimene R. Power generation by Stirling engine during fluidized bed combustion of wood pellets. *Combust Sci Technol*. 2019;191:263-274.

12. Weaver SP. Low Temperature Stirling Engine for Waste Heat Recovery from Distributed Power Sources. EPA Contract Number: EPD11045; 2011.

13. Obara S'y, ShunsukeKito AH, Sasaki S. Study on woody biomass Stirling cycle for cold region houses. *Int J Energy Res*. 2009;33(2):152-163.

14. Harrod J, Mago PJ, Luck R. Sizing analysis of a combined cooling, heating, and power system for a small office building using a wood waste biomass-fired Stirling engine. *Int J Energy Res*. 2012;36(1):64-74.

15. Damirchi H, Najafi G, Alizadehnia S, Mamat R, Nor Azwadi C, Azmi W, Noor M. Micro combined heat and power to provide heat and electrical power using biomass and gamma-type Stirling engine. *Appl Therm Eng*. 2016;103:1460-1469.

16. Angrisani G, Bizon K, Chirone R, et al. Development of a new concept solar-biomass cogeneration system. *Energy Convers Manag*. 2013;75:552-560.

17. Rokni M. Biomass gasification integrated with a solid oxide fuel cell and Stirling engine. *Energy*. 2014;77:6-18.

18. Ozawa A, Kudoh Y. Performance of residential fuel-cell-combined heat and power systems for various household types in Japan. *Int J Hydrog Energy*. 2018;43(32):15412-15422.

19. Chen W-L, Huang C-W, Li Y-H, Kao C-C, Cong HT. Biosyngas-fueled platinum reactor applied in micro combined heat and power system with a thermophotovoltaic array and Stirling engine. *Energy*. 2020;194:116862.

20. Lin J-C. Combination of a biomass fired updraft Gasifier and a Stirling engine for power production. *J Energy Resour Technol*. 2006;129(1):66-70.

21. Skorek-Osikowska A, Kotowicz J, Uchman W. Thermodynamic assessment of the operation of a self-sufficient, biomass based district heating system integrated with a Stirling engine and biomass gasification. *Energy*. 2017;141:1764-1778.

22. Aliabadi AA, Thomson MJ, Wallace JS, Tzanetakis T, Lamont W, Di Carlo J. Efficiency and emissions measurement of a Stirling-engine-based residential microcogeneration system run on diesel and biodiesel. *Energy Fuel*. 2009;23(2):1032-1039. https://doi.org/10.1021/ef800778g.

23. Farra N, Tzanetakis T, Thomson MJ. Experimental determination of the efficiency and emissions of a residential microcogeneration system based on a Stirling engine and fueled by diesel and ethanol. *Energy Fuel*. 2012;26(2):889-900.

24. Patel NK, Shah SN. *Biodiesel from plant oils*. In: Ahuja S, ed. *Food, energy, and water*. Amsterdam, The Netherlands: Elsevier; 2015:277-307.

25. Jahirul MI, Rasul MG, Chowdhury AA, Ashwath N. Biofuels production through biomass pyrolysis—a technological review. *Energies*. 2012;5:4952-5001.

26. Bridgwater AV. Review of fast pyrolysis of biomass and product upgrading. *Biomass Bioenergy*. 2012;38:68-94.

27. Nye MJ, Williamson TW, Deshpande WJ, et al. Conversion of used frying oil to diesel fuel by transesterification: preliminary tests. *J Am Oil Chem Soc*. 1983;60:1598-1601.

28. Prasad SB. Steam engine characteristics and theoretical performance. *Energy Convers Manag*. 1993;34(12):1323-1333.

29. Kalina J. Techno-economic assessment of small-scale integrated biomass gasification dual fuel combined cycle power plant. *Energy*. 2017;141:2499-2507.

30. Knudsen JK, Hottel HC, Sarofim AF, Wankat PC, Knaebel KS. Heat and mass transfer. In: Perry RH, Green DW, Maloney JO, eds. *Perry's chemical engineers' handbook*. 7th ed. New York, NY: McGraw-Hill; 1997;5-8:5-79.

31. Houshfar E, Khalil RA, Løvås T, Skreiberg Ø. Enhanced NOx reduction by combined staged air and flue gas recirculation in biomass grate combustion. *Energy Fuel*. 2012; 26:3003-3011.

32. Ente Nazionaleitaliano di unificazione. UNI-10389 Heating systems – Measurement on-site of combustion efficiency, 1994

33. Qnergy Ltd. PCK80.1System Integration Guide; 2017.